Image Based Finite Element Analysis of 3D-Orthogonal Carbon-Carbon (C/C) Composite

Rajneesh Sharma, Puneet Mahajan[1], and Ramesh Kumar Mittal

Abstract— Carbon–carbon (c/c) composites have low density, high stiffness and retain their properties at high temperature. The manufactured composite has significant internal damage like, voids, matrix cracking and debonding at interfaces due to the mismatch in thermal stresses induced during manufacturing process. Also there is some distortion of the cross-section of the fibre bundles. All these imperfections influence the mechanical properties of the composite. A computed tomography (CT) scan is performed on a composite specimen and 3D image is reconstructed. Unit cell is taken form the reconstructed image and is analyzed by using finite element (FE) method. The manufacturing imperfections are included in the FE mesh. Asymptotic homogenization along with periodic boundary conditions is used to determine the mechanical properties. Results obtained are compared to those available in the literature.

***Index Terms*— Carbon/carbon composites; X-ray tomography; Reconstruction; IBFEM**

I. Introduction

Carbon/carbon composites (C/C) are well known high-performance materials in aerospace industry. They are in demand in industry, due to their high performance in thermo structural application, such as rocket nozzles [10] or airplane brakes, and their market is in appreciable extension. Therefore, determining their thermo-mechanical properties is essential for safe design and operation of components. Prediction of the mechanical properties of these composites is very advantageous as costs of performing expensive and time-consuming experiments can be substantially reduced. Also analysis of structures using these materials requires that the non-homogeneous material be replaced by an equivalent homogeneous material (EHM).

Asymptotic homogenization is one of the many available methods to determine the properties of this EHM [9]. In this homogenization technique it is assumed that the composite is a periodic structure can be replicated by translating or reflecting a unit cell. The implementation of this method requires finite element analysis of the unit cell with periodic boundary conditions imposed on it and has been used by Rao et al. [9] to get the equivalent homogenized properties for different architectures of C/C composites. However, the structural models used there were based on the ideal material structure which differs from the real one as follows;

1. Real fibers differ from the ideal one in cross-section and alignment. These defects termed as global volume imperfections, appear in the composite before heat treatment.
2. Real structure also contains defects like voids and cracks which originate during heat treatment. These defects are termed as local imperfections.

The voids and cracks are the main dominating imperfections in carbon composite and have significant effect on composite properties. The aim of the present study is to determine mechanical properties for advanced reinforced c/c composite structures where global and local imperfections are included in the model. The first and unique method is based on the use of an image-based route to acquire FE models from real structure [2]. This is achieved by reconstructing 3D image of the composite unit cell from high resolution 2D images. Similar approaches have been also adopted in literature for modelling nuclear graphite [7], dental structures [5], carbon fibre-epoxy laminates [6], carbon-carbon composites [3], and quantification of bone tissue [15].

A comparative study of unit cell based and image based finite element method (IBFEM) with experiments is presented by Ali et al. [1] for 2D woven c/c composite. It is concluded that the predictions of IBFEM are closer to the experiments.

In the present work, 3D orthogonal hybrid composite, containing rectangular fibre bundles in x and y directions and circular bundles in z direction is analyzed. The material structure of the composite is reconstructed from the 2D images obtained from the x-ray computed tomography. A unit cell is cropped from the reconstructed structure and analysed by using asymptotic homogenization technique with periodic boundary conditions. The comparison of the properties from IBFEM to the conventional unit-cell based finite element method is presented. The reconstruction and formulation of the problem are discussed in the following sections.

II. Composite Material Image Reconstruction

The x-ray computed tomography for image reconstruction is a non-destructive and fully automated method [4,14]. The 3D

Manuscript received March 11, 2010

Rajneesh sharma, research scholar, Applied Mechanics Department, Indian Institute of Technology Delhi, New Delhi-16, India

[1] Corresponding author

Puneet Mahajan, Professor, Applied Mechanics Department, Indian Institute of Technology Delhi, New Delhi-16, India, (e-mail: mahajan@am.iitd.ernet.in). Tel.: +91 11 26591229; fax: +91 11 26581119

Ramesh Kumar Mittal, Professor, , Applied Mechanics Department, Indian Institute of Technology Delhi, New Delhi-16, India

ISBN: 978-988-18210-7-2
ISSN: 2078-0958 (Print); ISSN: 2078-0966 (Online)

reconstruction of image by using x-ray tomography can be done in three steps, as illustrated in Fig.1, and discussed as follows.

1. During the acquisition the object rotates over 180 or 360 degrees with a fixed small step rotation. At each angular position a shadow image or transmission image is acquired. The cone beam acquisition system saves all these projection images as 16 bit TIFF files on the disk.
2. Reconstruction is done from 16-bit TIFF shadow images to generate virtual slices. A raw data of the cross section in terms of a floating point matrix is then generated.
3. The absorption information of x-ray in the floating point matrix is converted to a grey scale image.

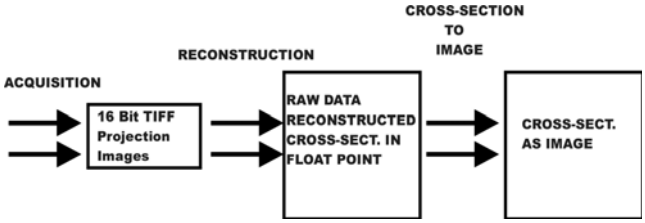

Figure 1: Acquisition to the final reconstructed cross section of image

This reconstructions technique is integrated in "SkyScan-1172" [14] desktop x-ray micro-tomograph and used in present study. A sample of "9x9x9 mm^3" is scanned by using x-ray micro-tomograph at different energy levels and the best resolution is found at 80kV. The bundles of the composite sample contained 48000 PAN-based carbon fibers embedded in carbonized matrix [9]. The scanning details are given in Table 1.

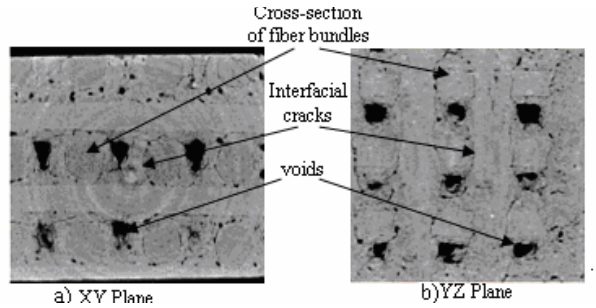

Figure 2: Reconstructed 2D slices with voids and cracks for 3D orthogonal c/c composite.

The reconstructed 2D images from CT for 3D-orthogonal composite are shown in Fig.2. The voids and cracks are clearly distinguishable in the 2D images.

The presence of the voids is observed at each fiber junction and they are nearly periodically distributed in the composite. The cross-sections of the fiber bundles are distinguishable by eye in these 2D images, but it is still difficult to recognize them by using grey scale, as the grey levels of matrix and fiber bundles are nearly same.

Therefore a manual segmentation process is carried out for the reconstruction of the fiber bundles. Fig.3 shows the methodology of the reconstruction of the fiber bundles along with segmentation details. Commercial software "Simpleware" [13] is used for the 3D reconstruction of the composite. The procedure of reconstruction for z-directional fiber bundles is discussed in the following.

1. Recognize and mark the cross-sections of bundles on each 2D image of XY plane which help in the creation longitudinal sections in other two planes (XZ and YZ).
2. Longitudinal sections obtained in XZ and YZ planes have the rough edges; therefore smooth the edges on each slice.
3. Recheck the cross-section in XY plane to ensure that the extra removal has not occurred in cross-section and improve it if required.
4. Repeat this procedure 2-3 times to have an enhanced reconstruction of fiber bundle in z-direction.

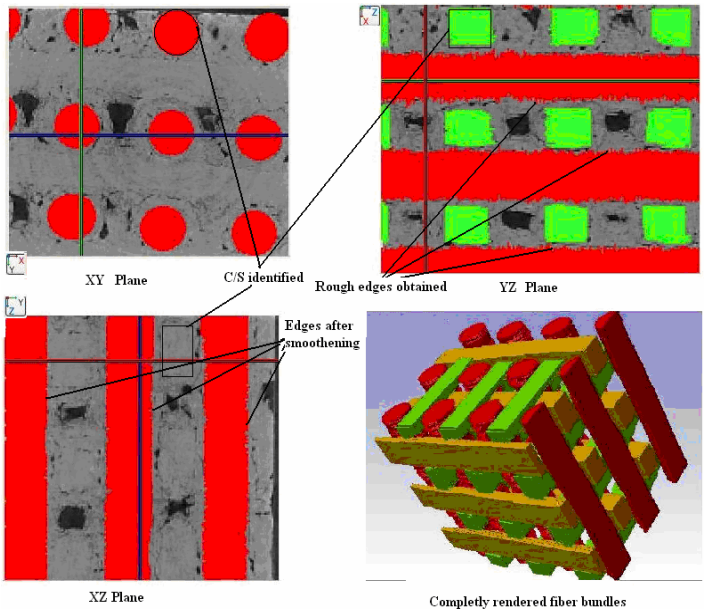

Figure 3: Segmentation and 3D Reconstruction of fibres in 3D-orthogonal c/c composite

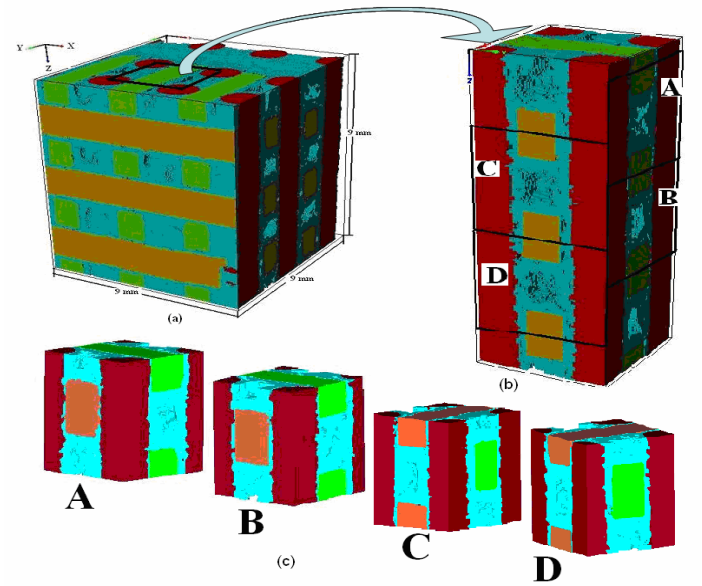

Figure 4: (a) 3D reconstructed image of composite including imperfections.
(b) Cropped unit cell region along z-direction
(c) Four cropped unit cells

Other directional fiber bundles can also reconstructed by using above steps. After the reconstruction of the fiber bundles next step is to reconstruct the matrix with voids and cracks included in it. Voids and cracks are obtained in a new

ISBN: 978-988-18210-7-2
ISSN: 2078-0958 (Print); ISSN: 2078-0966 (Online)

Table 1: CT parameters used for 3D composite

X-ray tube: energy/intensity		Radiograph acquisition		Reconstruction area		
Voltage (kV)	Current (mA)	Angular displacement (º)	Exposure time (ms)	Pixel size (μm)	Width (pixels)	Height (pixels)
80	100	0.30	1178	6.936	900	900

Table 2: Unit cell properties for a 3D composite

Sample	Size	Volume of fibres in x-direction	Volume of fibres in y-direction	Volume of fibres in z-direction	Matrix volume	Fibre fraction %	Void fraction %
A	2.70x2.75x2.90	3.573	3.446	4.566	7.869	53.80	9.65
B	2.65x2.70x2.85	3.87	3.564	4.197	7.340	56.90	8.45
C	2.75x2.95x2.95	3.507	4.125	5.581	8.741	55.21	8.26
D	2.75x2.70x2.85	3.961	3.471	4.573	7.342	56.73	8.57

collector by controlling the gray scale threshold values such that it will represent all the required features. Again, a new collector is created for the matrix which contains all gray scale levels (0-255). The matrix is obtained by subtracting the voids, cracks and fiber bundles from it. The 3D reconstructed image of the composite with all the imperfections is shown in Fig.4. Finally the 3D voxel based finite element mesh is obtained from this image of the composite. The mesh obtained has 5,078,622 nodes and 4,778,587 tetrahedral elements. As the number of elements is large and not easy to handle with the present computational facilities, the unit cell based technique is considered by taking four RVE's from the scanned composite as shown in the Fig.4.

When the unit cell is cropped from the real material structure the artifacts like voids, cracks, alignment of fiber bundles and volume fractions are not uniform in the composite at micro scale. In order to get an idea of the variation of the properties in the real material structure, two consecutive cells are taken from x-direction and two consecutive cells from y-direction, such that y-directional cells overlap x-direction cells by 50% as shown in Fig.4. For the homogenization of the real composite structure, it is assumed that the structure is reliably replicated by repeating each unit cell in orthogonal directions.

Since, the methodology used the image based route to acquire the real material structure for finite element analyses is referred as Image Based Finite Element Method (IBFEM) and discussed in next section.

III. Modeling

The asymptotic homogenization method was next used on the image based unit cells obtained above to obtain equivalent homogeneous properties. It is assumed that the each equivalent material structure for composite can be represented reliably by reflecting the unit cell in three orthogonal directions and subsequently translating it. This requires the use of reflection periodic boundary conditions. The details of the unit cells are given in Table 2. It is observed that the voids are nearly uniformly distributed and of the same size, and are considered as periodic. The final properties are obtained by volume averaging of the results obtained from the four unit cells shown in Fig. 4. The homogenization and boundary conditions considered are discussed in next section.

A. Homogenization

The technique used to replace heterogeneous material with an equivalent homogenized material is known as homogenization. Asymptotic homogenization is one way of homogenization and considered in the present study. The details of the derivation are given by Rao et al. [8]. The constitutive equation for asymptotic homogenization is given as below.

$$\left\langle \sigma_{ij} \right\rangle = C^{H}_{ijkl}\left(\varepsilon_{ij}\right)\varepsilon_{kl} \quad (1)$$

where C^{H}_{ijkl} are the equivalent homogenized stiffness coefficients, ε_{kl} are the volume averaged strains and $\left\langle \sigma_{ij} \right\rangle$ is the volume averaged stress given by following expression:

$$\left\langle \sigma_{ij} \right\rangle = \frac{1}{V_e}\int_{v_e} \sigma_{ij}\, dv_e \quad (2)$$

V_e is the volume of the element. The stiffness coefficients can be related to the nine engineering constants for an orthotropic material [8].

The stiffness coefficients are determined by applying six independent load cases with respective boundary conditions as mentioned above in equations 1-4. The loading in each case is in the form of micro-strains and as given below.

$$\begin{Bmatrix} e_{11} \\ e_{22} \\ e_{33} \\ e_{23} \\ e_{13} \\ e_{12} \end{Bmatrix} = \begin{Bmatrix} 1 \\ 0 \\ 0 \\ 0 \\ 0 \\ 0 \end{Bmatrix}; \begin{Bmatrix} e_{11} \\ e_{22} \\ e_{33} \\ e_{23} \\ e_{13} \\ e_{12} \end{Bmatrix} = \begin{Bmatrix} 0 \\ 1 \\ 0 \\ 0 \\ 0 \\ 0 \end{Bmatrix}; \begin{Bmatrix} e_{11} \\ e_{22} \\ e_{33} \\ e_{23} \\ e_{13} \\ e_{12} \end{Bmatrix} = \begin{Bmatrix} 0 \\ 0 \\ 1 \\ 0 \\ 0 \\ 0 \end{Bmatrix}; \begin{Bmatrix} e_{11} \\ e_{22} \\ e_{33} \\ e_{23} \\ e_{13} \\ e_{12} \end{Bmatrix} = \begin{Bmatrix} 0 \\ 0 \\ 0 \\ 1 \\ 0 \\ 0 \end{Bmatrix}; \begin{Bmatrix} e_{11} \\ e_{22} \\ e_{33} \\ e_{23} \\ e_{13} \\ e_{12} \end{Bmatrix} = \begin{Bmatrix} 0 \\ 0 \\ 0 \\ 0 \\ 1 \\ 0 \end{Bmatrix}; \begin{Bmatrix} e_{11} \\ e_{22} \\ e_{33} \\ e_{23} \\ e_{13} \\ e_{12} \end{Bmatrix} = \begin{Bmatrix} 0 \\ 0 \\ 0 \\ 0 \\ 0 \\ 1 \end{Bmatrix} \quad (3)$$

For example to obtain the first column of the stiffness matrix e_{11} is kept non zero and other strains are set equal to zero. In this way all the components of the stiffness matrix are obtained by applying loadings one by one. Final properties of

ISBN: 978-988-18210-7-2
ISSN: 2078-0958 (Print); ISSN: 2078-0966 (Online)

composite are obtained as the volume averaged of the four unit cells.

B. Boundary condition

The boundary conditions are derived by the principle of symmetries, which states that symmetrical stimuli result in symmetric response and anti-symmetric stimuli produce anti-symmetric response [12]. Further, in order to apply the reflection symmetries about x, y, z planes, one has to consider individual load cases expressed in terms of micro stresses (σ_{11}, σ_{22}, σ_{33}, τ_{23}, τ_{13}, τ_{12}). The advantage of reflection boundary conditions is that they maintain the continuity of the fiber bundles at the plane of symmetry.

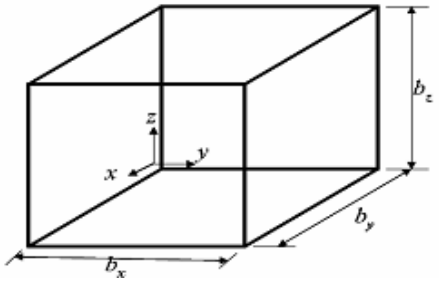

Figure: 6 unit cell for boundary conditions

1) Under normal stresses (σ_{11}, σ_{22}, σ_{33})*:*

The boundary conditions for two opposite faces of a unit cell are given by Equ.(1), when normal loadings are applied one by one. When σ_{11} is applied then e_{11} is associated with face $x=b_x$ and e_{22}, e_{33} are kept free. Similarly, for σ_{22} and σ_{33}, e_{22} and e_{33} are the respective degrees of freedom associated with $y=b_y$ and $z=b_z$ and other strains are kept free.

$$\left.\begin{aligned} u\big|_{x=0} &= 0 \;\;\&\;\; u\big|_{x=b_x} = b_x\varepsilon_{11} \\ v\big|_{y=0} &= 0 \;\;\&\;\; v\big|_{y=b_y} = b_y\varepsilon_{22} \\ w\big|_{z=0} &= 0 \;\;\&\;\; w\big|_{z=b_z} = b_z\varepsilon_{33} \end{aligned}\right\} \quad (4)$$

where u, v and w are the degree of freedom at each node in x, y and z direction respectively.

2) Under shear stresses (τ_{23}, τ_{13}, τ_{12}):

Shear stress conditions are slightly more complicated than those for direct stresses. For the reflection symmetry, one of the three shear stress components is symmetric and other two are anti-symmetric. The boundary conditions for the unit cell under τ_{23}, τ_{13} and τ_{12} when considered one by one are given as below by equations (2),(3) and (4) respectively.

$$\left.\begin{aligned} u\big|_{x=0} &= 0 & u\big|_{x=b_x} &= 0 \\ u\big|_{y=0} &= w\big|_{y=0} = 0 & u\big|_{y=b_y} &= w\big|_{y=b_y} = 0 \\ u\big|_{z=0} &= v\big|_{z=0} = 0 & u\big|_{z=b_z} &= 0 \;\&\; v\big|_{z=b_z} = b_z\gamma_{23} \end{aligned}\right\} \quad (5)$$

$$\left.\begin{aligned} v\big|_{x=0} &= w\big|_{x=0} = 0 & v\big|_{x=b_x} &= w\big|_{x=b_x} = 0 \\ v\big|_{y=0} &= 0 & v\big|_{y=b_y} &= 0 \\ u\big|_{z=0} &= v\big|_{z=0} = 0 & u\big|_{z=b_z} &= b_z\gamma_{13} \;\&\; v\big|_{z=b_z} = 0 \end{aligned}\right\} \quad (6)$$

$$\left.\begin{aligned} v\big|_{x=0} &= w\big|_{x=0} = 0 & v\big|_{x=b_x} &= w\big|_{x=b_x} = 0 \\ u\big|_{y=0} &= w\big|_{y=0} = 0 & u\big|_{y=b_y} &= b_y\gamma_{12} \;\&\; w\big|_{y=b_y} = 0 \\ w\big|_{z=0} &= 0 & w\big|_{z=b_z} &= 0 \end{aligned}\right\} \quad (7)$$

Table 3: Effective properties of fibre bundle and matrix GPa

Material	E_{11}	$E_{22}=E_{33}$	$G_{12}=G_{13}$	G_{23}	$\nu_{12}=\nu_{13}$	ν_{23}
Fibre bundle	240	19	23.63	7	0.2	0.34
Matrix	19	-	7.92	-	0.2	-

IV. Results and Discussion

Rao et al. [9] have considered the case of perfect bonding between the fibre and the matrix and compared the results of the unit cell approach with the experimental results. In the present work, values of stiffness of the fibre bundle and matrix stiffness were taken same as reported by Rao et al. [8] and are given in Table 3. The fibre bundles were considered to be transversely isotropic while matrix was taken as isotropic.

The predicted engineering stiffness properties of the unit cells are presented in Table 4. It is noted that the variation in the properties is 10-20% among the unit cells. The E_{11} varies about 9%, whereas for E_{22} and E_{33} is about 13% among the unit cells. The deviation of ν_{12} and ν_{13} is about 10%, while ν_{23} is same for cases (B, C, D) and differs by 3% for case (A). The difference in shear modulus is in the rage of 15 to 20%. This variation is due to the change in the volume fraction and orientation of fibres, voids and cracks in the each unit cells. The mechanical properties are further volume averaged to take into account the variations in the properties of unit cells of the composite. The volume averaged properties of the unit cells are presented and compared with Rao et al. [9] in the Table 5. Here it is observed that the composite is orthotropic and no more transversely isotropic as reported in the literature [9]. This difference is because Rao et al. [9] assumed that the material structure is ideal and the fibre volume fraction is uniformly distributed in all directions. The imperfections like voids and cracks were taken symmetric in all directions for characterization of the composite. Where as, in the present study the realistic material structure is considered with all manufactured artefacts. The significant degradation in the mechanical properties of composite is also observed from Table 5.

Table 4: Stiffness properties in GPa for unit cells A, B, C, D.

Sample	E_{11}	E_{22}	E_{33}	ν_{23}	ν_{13}	ν_{12}	G_{12}	G_{13}	G_{23}
A	51.81	50.64	56.73	0.069	0.064	0.075	8.53	8.14	7.89
B	56.56	55.17	59.13	0.071	0.068	0.073	9.18	8.82	8.46
C	53.54	58.29	65.84	0.071	0.068	0.080	10.65	9.79	9.19
D	56.66	55.78	63.69	0.071	0.060	0.072	9.20	9.04	8.30

ISBN: 978-988-18210-7-2
ISSN: 2078-0958 (Print); ISSN: 2078-0966 (Online)

Table 5: Stiffness properties in GPa from element volume average

Method	E_{11}	E_{22}	E_{33}	ν_{23}	ν_{13}	ν_{12}	G_{12}	G_{13}	G_{23}
IBFEM	54.6	55.1	61.5	0.07	0.07	0.08	9.42	8.97	8.47
Rao et al.	56.52	56.52	62.18	0.08	0.08	0.088	10.4	10.9	10.9

V. Conclusions

X-ray tomography is a very powerful tool for material characterization and is successfully used for the reconstruction of the c/c composite in the present study. Classical x-ray tomography does not give enough contrast between two phases of carbon-carbon composite, as the difference between densities of the fiber and matrix is very small. However through manual intervention it is possible to differentiate between fiber bundle and matrix interfaces.

1) Imperfections like misalignment, c/s warping, size, shape and distribution of voids and cracks are also very useful data for mechanical characterization of composite. Misalignment and warping have been approximately modeled.
2) It is observed that the voids are periodically and nearly equally distributed through out the composite. From 3D reconstruction a realistic voxel based finite element mesh is obtained, which includes almost all the imperfections presented in the composite. The mesh obtained is very fine and therefore unit cell approach is used in present study. Assuming periodic boundary conditions a unit cell is analyzed to determine the homogenous properties of the composite. Next four different adjacent regions in the same specimen is analyzed. Due to different alignments of fiber bundle cross-section, there are variations up to 10% in Young's modulii between different unit cells. The shear modulii particularly G_{12} for sample "C" showed higher variation due to void distribution.
3) Each of the unit cells used predicted the mechanical properties to be orthotropic. A comparison with properties obtained from perfectly bonded composite show that imperfections produce considerable degradation in the properties.

References

[1] J. Ali, C. Berre, and P.M. Mummery, "Image based modelling of stressstrain behaviour in carbon/carbon composites". *Energy Materials: Materials Science and Engineering for Energy Systems,* 2006. 1: p. 179-186.

[2] J. Ali, J. K. Farooqi, D. Buckthorpe, A. Cheyne and P. Mummery, "Comparative study of predictive FE methods for mechanical properties of nuclear composites". *Journal of Nuclear Materials*, 2009. 383(3): p. 247-253.

[3] O. Coindreau, G. Vignoles, and P. Cloetens, "Direct 3D microscale imaging of carbon-carbon composites with computed holotomography". *Nuclear Instruments and Methods in Physics Research Section B: Beam Interactions with Materials and Atoms*, 2003. 200: p. 308-314.

[4] M. Kosek, and P. Sejak, "Visualization of voids in actual C/C woven composite structure". *Composites Science and Technology.*, 2009. 69: p. 1465–1469.

[5] P. Magne, "Efficient 3D finite element analysis of dental restorative procedures using micro-CT data". *Dental Materials*, 2007. 23(5): p. 539-548.

[6] J. Martín-Herrero, and C. Germain, "Microstructure reconstruction of fibrous C/C composites from X-ray microtomography". *Carbon*, 2007. 45(6): p. 1242-1253.

[7] N. More, B. Bassecathalinat, C. Baquey, F. Lacroix, D. Ducassou, "Application of novel techniques of medical imaging to the non-destructive analysis of carbon-carbon composite materials". *Nuclear Instruments and Methods in Physics Research*, 1983. 214(2-3): p. 531-536.

[8] M. V. Rao, P. Mahajan, and R.K. Mittal, "Effect of architecture on mechanical properties of carbon/carbon composites". *Composite Structures*, 2008. 83(2): p. 131-142.

[9] M. V. Rao, "Mechanical properties of multidirectional carbon -carbon composites" *PhD thesis, Applied mechanics department, Indian Institute of Technology Delhi, New delhi-16 India*, 2008

[10] J. K. Rebelo, M. Hofmann, and S. Schmidt, "Non-destructive testing of satellite nozzles made of carbon fibre ceramic matrix composite, C/SiC". *Materials Characterization*, 2007. 58(10): p. 922-927.

[11] S. Li, "Boundary conditions for unit cells from periodic microstructures and their implications". *Composites Science and Technology*, 2008, 68: p. 1962-1974.

[12] Simpleware Ltd., Innovation Centre, Rennes Drive, Exeter, EX4 4RN, UK.

[13] SkyScan 1172, DRDO facility at SASE, Manali, India.

[14] M. Stiller, A. Rack, S. Zabler, J. Goebbels, O. Dalügge, S. Jonscher, C. Knabe, "Quantification of bone tissue regeneration employing β-tricalcium phosphate by three-dimensional non-invasive synchrotron micro-tomography - a comparative examination with histomorphometry". *Bone*. 2009. 44(4): p. 619-628.

[15] G. L. Vignoles, "Image segmentation for phase-contrast hard X-ray CMT of C/C composites". *Carbon*, 2001. 39(2): p. 167-173.

ISBN: 978-988-18210-7-2
ISSN: 2078-0958 (Print); ISSN: 2078-0966 (Online)